Proceedings of NHTC'00
34th National Heat Transfer Conference
August 20-22, 2000, Pittsburgh, Pennsylvania, USA

NHTC2000-12268

THE EFFECT OF WORKING FLUID INVENTORY ON THE PERFORMANCE OF REVOLVING HELICALLY-GROOVED HEAT PIPES

R. Michael Castle
Scott K. Thomas*
Department of Mechanical and Materials Engineering
Wright State University
Dayton, Ohio 45435

Kirk L. Yerkes
Air Force Research Laboratory (PRPG)
Wright–Patterson AFB,
Dayton, Ohio 45433–7251

ABSTRACT

The results of a recently completed experimental and analytical study showed that the capillary limit of a helically–grooved heat pipe (HGHP) was increased significantly when the transverse body force field was increased. This was due to the geometry of the helical groove wick structure. The objective of the present research was to experimentally determine the performance of revolving helically–grooved heat pipes when the working fluid inventory was varied. This report describes the measurement of the geometry of the heat pipe wick structure and the construction and testing of a heat pipe filling station. In addition, an extensive analysis of the uncertainty involved in the filling procedure and working fluid inventory has been outlined. Experimental measurements include the maximum heat transport, thermal resistance and evaporative heat transfer coefficient of the revolving helically–grooved heat pipe for radial accelerations of $|\vec{a}_r|$ = 0.0, 2.0, 4.0, 6.0, 8.0, and 10.0-g and working fluid fills of G = 0.5, 1.0 and 1.5. An existing capillary limit model was updated and comparisons were made to the present experimental data.

NOMENCLATURE

a adiabatic length near the evaporator end cap, m
α radial acceleration, m/s^2
A_e surface area in the evaporator section, $\pi r_v^2 L_e$, m^2
$A_{\rm gr}$ cross–sectional area of a groove, m^2
b adiabatic length near the condenser end cap, m
C_p specific heat at constant pressure, J/(kg-K)
D_o tube outside diameter, m
$D_{\rm vs}$ diameter of the heat pipe vapor space, m
G Ratio of liquid volume to total groove volume, $V_l/V_{\rm gr}$
h groove height, m
h_e local heat transfer coefficient in the evaporator section, $Q_t/A_e(T_w - T_a)$, W/m^2-K
I heater current, A
L_a adiabatic length, m
L_c condenser length, m
L_e evaporator length, m
$L_{\rm gr}$ helical groove length, m
L_t total heat pipe length, m
m_d mass of working fluid dispensed by the filling station, kg
m_l mass of liquid, kg
m_t total mass of working fluid inventory, kg
m_v mass of vapor, kg
$\dot{m}_c$ coolant mass flow rate, kg/s
$N_{\rm gr}$ number of grooves
p helical pitch, m
$Q_{\rm cap}$ capillary limit, W
$Q_{\rm in}$ heat input at the evaporator, W
Q_t heat transported, $\dot{m}_c C_p(T_{\rm out} - T_{\rm in})$, W
r_h radius of the helix, m
r_v radius of the heat pipe vapor space, m
R radius of curvature, m
$R_{\rm th}$ thermal resistance, $(T_{\rm eec} - T_{\rm cec})/Q_t$, K/W

* Author to whom correspondence should be directed.

s coordinate along the centerline of the heat pipe, m
t_w tube wall thickness, m
T_a adiabatic temperature, K
T_{cec} condenser end cap temperature, K
T_{eec} evaporator end cap temperature, K
T_{in} calorimeter inlet temperature, K
T_{out} calorimeter outlet temperature, K
T_{sat} saturation temperature, K
T_w outer wall temperature, K
v_l, v_v specific volume of liquid and vapor, m^3/kg
V heater voltage
V_{gr} volume of the grooves, m^3
V_{vs} vapor space volume, m^3
w width along the bottom of the groove, m
x distance from the evaporator end cap, m
Δ uncertainty
θ_1, θ_2 angles from the sides of the groove to vertical, rad
ϕ helix angle, rad

INTRODUCTION

Helically–grooved heat pipes (HGHPs) have potential applications in the thermal management of rotating equipment such as aircraft alternators, large–scale industrial electric motors, and spinning satellites. In two recent studies (Klasing et al., 1999; Thomas et al., 1998), the performance of revolving HGHPs was investigated. It was found that the capillary limit increased with the strength of the acceleration field perpendicular to the heat pipe axis. In order to move HGHPs closer to application, knowledge must be gained concerning the sensitivity of the capillary limit to working fluid fill amount, since variations in the fill amount are inevitable during the manufacture of these devices. Very few studies were available concerning the effect of working fluid fill on the performance of axially–grooved heat pipes, but those found have been outlined below. In addition, synopses of the two aforementioned studies on revolving HGHPs have also been provided.

Brennan et al. (1977) developed a mathematical model to determine the performance of an axially–grooved heat pipe which accounts for liquid recession, liquid–vapor shear interaction and puddle flow in a 1-g acceleration environment. The model considered three distinct flow zones: the grooves unaffected by the puddle, the grooves that emerge from the puddle, and the grooves that are submerged by the puddle. The model for the puddle consisted of satisfying the equation of motion for the puddle and the continuity equation at the puddle–groove interface, and was solved by a fourth–order Runge–Kutta integration method with self–adjusting step sizes. The assumptions made by the model for the puddle were uniform heat addition and removal with a single evaporator and a single condenser section, and one–dimensional laminar flow in the puddle. The transport capability of the grooves unaffected by the puddle and the grooves extending beyond the puddle were approximated by a closed–form solution with laminar liquid and vapor flow. The working fluids used for the experiment were methane, ethane and ammonia. Brennan et al. (1977) stated that the mathematical model agreed well with the experimental data for ideally filled and overfilled heat pipes, but some differences were noted for underfilled heat pipes. In general, it was found for ideally filled heat pipes the predicted transported heat was higher than that measured. Also, this discrepancy was more significant for lower operating temperatures. In addition, it was found during the experiments that the maximum transported heat increased with fill volume.

Vasiliev et al. (1981) performed a series of experiments on an aluminum axially–grooved heat pipe which was overfilled and ideally filled. The width and height of the grooves were w = 0.123 mm and h = 0.7 mm, respectively, with an overall heat pipe length of L_t = 80.0 cm. The working fluids were acetone and ammonia. Vasiliev et al. showed that the temperature difference from the evaporator to the adiabatic regions increased at a much slower rate with increasing overfills. This was attributed to a thin film of liquid emerging from the overfill pool wetting the upper grooves. Vasiliev et al. stated that this thin film was lifted over the grooves by capillary forces due to microroughness on the groove surface. A mathematical model was developed for low temperature axially–grooved heat pipes to estimate heat pipe performance for 0-g and 1-g applications. The mathematical model was a set of boundary–value problems applied to each groove and was solved by a numerical iteration method. The model was based on pressure balance equations and mass continuity written for a single groove. The temperature of the vapor in the adiabatic region was an input parameter, and the vapor pressure gradient was assumed to be one–dimensional. In addition, the liquid–vapor shear stress was assumed to be constant, and the starting liquid film thickness was of the same order of magnitude as the groove microroughness. Very good agreement was reported between the mathematical model and experimental transported heat results for ideally filled and overfilled heat pipes under gravity.

Thomas et al. (1998) presented experimental data obtained from a helically–grooved copper heat pipe which was tested on a centrifuge table. The heat pipe was bent to match the radius of curvature of the table so that uniform transverse (perpendicular to the axis of the heat pipe) body forces field could be applied along the entire length of the pipe. The steady–state performance of the curved heat pipe was determined by varying the heat input (Q_{in} = 25 to 250 W) and centrifuge table velocity (radial acceleration $|\vec{a}_r|$ = 0.01 to 10-g). It was found that the capillary limit increased by a factor of five when the radial acceleration increased from $|\vec{a}_r|$ = 0.01 to 6-g due to the geometry of the helical grooves. A model was developed to calculate the capillary limit of each groove in terms of centrifuge table angular velocity, the geometry of the heat pipe and the grooves, and the temperature–dependent

working fluid properties. The agreement between the model and the experimental data was satisfactory.

Klasing et al. (1999) developed a mathematical model to determine the operating limits of a revolving helically–grooved straight heat pipe. The capillary limit calculation required an analysis of the total body force imposed by rotation and gravity on the liquid along the length of the helical grooves. The boiling and entrainment limits were calculated using methods described by Faghri (1995). It was found that the capillary limit increased significantly with rotational speed due to the helical geometry of the heat pipe wick structure. The maximum heat transport was found to be a function of angular velocity and tilt angle from horizontal. In addition, a minimum value of angular velocity was required to obtain the benefits of the helical groove geometry.

The first objective of the present study was to determine the sensitivity of the performance of revolving HGHPs to the working fluid fill amount. This required a precise knowledge of the geometry of the heat pipe and helical grooves. In addition, a precision filling station was constructed and calibrated to determine the uncertainties involved in the filling procedure. The copper–ethanol heat pipe was tested on a centrifuge table at Wright–Patterson AFB (AFRL/PRPG) to determine the capillary limit, thermal resistance and evaporative heat transfer coefficient for fill ratios of G = 0.5, 1.0 and 1.5, and radial accelerations of $|\vec{a}_r|$ = 0.01, 2.0, 4.0, 6.0, 8.0 and 10.0-g. The second objective of the present study was to improve the existing analytical capillary limit model developed by Thomas et al. (1998) using the above–mentioned geometric measurements and by using improved equations for the working fluid properties.

Determination of Heat Pipe Working Fluid Inventory

The objective of this analysis was to determine the working fluid inventory of a HGHP, which consists of the mass of liquid in the grooves and the mass of vapor in the vapor space. Since the heat pipe is a closed container under saturation conditions, the total mass of working fluid in the heat pipe is given by

$$m_t = m_v + m_l = \frac{V_{\rm vs}}{v_v} + \frac{GV_{\rm gr}}{v_l} \tag{1}$$

where $G = V_l/V_{\rm gr}$ is the ratio of the volume of liquid to total groove volume. The volume of the vapor space is

$$V_{\rm vs} = \frac{\pi}{4} D_{\rm vs}^2 L_t + V_{\rm gr}(1-G) \tag{2}$$

The second term in eqn. (2) accounts for the increase or decrease in the vapor space volume when the parameter G is varied. The total volume of the grooves is

$$V_{\rm gr} = L_{\rm gr} N_{\rm gr} A_{\rm gr} \tag{3}$$

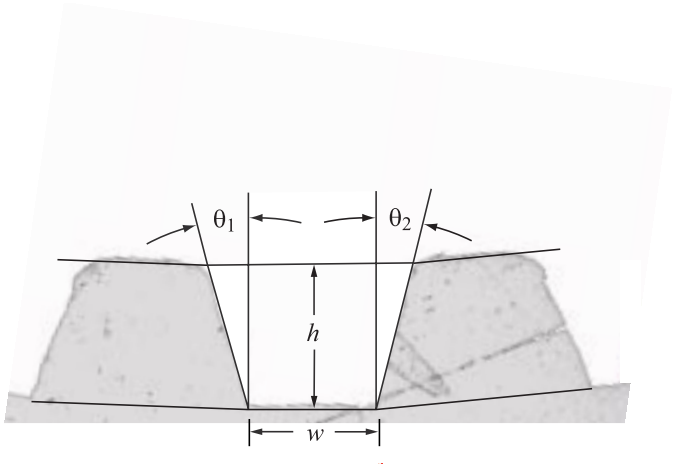

Figure 1. Photomicrograph of the helical groove geometry.

A cross–sectional view of a typical helical groove in the experimental test article is shown in Fig. 1. The cross–sectional area of the trapezoidal groove accounts for the differing side angles.

$$A_{\rm gr} = wh + \frac{1}{2}h^2(\tan\theta_1 + \tan\theta_2) \tag{4}$$

The total length of each groove is

$$L_{\rm gr} = L_t \left[\left(\frac{2\pi r_h}{p} \right)^2 + 1 \right]^{\frac{1}{2}} \tag{5}$$

The radius of the helix is given by

$$r_h = \frac{1}{2}(D_{\rm vs} + h) \tag{6}$$

The helical pitch is the distance through which the helix makes one revolution around its radius.

$$p = \frac{2\pi(s - s_1)}{(\phi - \phi_1)} \tag{7}$$

The helix angle ϕ corresponds to s, which is the distance traveled along the centerline of the heat pipe.

In order to calculate the working fluid inventory for the HGHP, measurements of the appropriate geometric parameters were made. In addition, an extensive uncertainty analysis was performed to determine the uncertainties of both the measured and calculated variables used in finding the working fluid inventory.

The physical variables given in eqn. (4) for the cross–sectional area of the grooves have been measured. A sample of the HGHP container was set in an epoxy resin mold, polished, and examined under a microscope with 50× magnification. Computer software was used to make bitmap pictures of

ten different grooves and a microscopic calibration scale. These pictures were then analyzed to determine the geometric values shown in Fig. 1. Since the corners at the top of the land between grooves were not well defined, a special procedure was established to determine the geometry of the grooves. First, lines were drawn along the bottom and sides of each groove. Then, a line was drawn across the bottom of the land between grooves, as shown in Fig. 1. This line was then transposed to the top of the land. The intersections between this line and the lines along the sides of the groove were defined as the upper corners of the groove. Note that the two lines along the land tops are at different angles due to the radius of curvature of the heat pipe container. The angles θ_1 and θ_2, and the height and width of the groove h and w were found using a bitmap picture of the microscopic calibration scale as described by Castle (1999).

An optical comparator was used to determine the vapor space diameter of the heat pipe container sample. The cross hairs of the optical comparator were carefully aligned with the top of the land between grooves on the left edge of the pipe. The comparator table was then moved until the land tops on the right edge of the pipe were aligned with the cross hairs. The diameter of the heat pipe vapor space was the distance of the table movement.

The helical groove pitch was found using a vertical milling machine and an angular displacement transducer. The heat pipe container material was originally 1 m long. Approximately one-half was used to form the heat pipe, and the other half was used to determine the pitch. The rotation angle $(\phi - \phi_1)$ and the corresponding distance along the centerline of the heat pipe $(s - s_1)$ has been found as shown in Fig. 2(*a*). A heat pipe holding device was constructed from two angle aluminum uprights mounted to the table of a vertical milling machine. Precision alignment blocks were attached to the undersides of the uprights to engage one of the grooves in the milling machine table for improved alignment. Nylon bushings were placed in the uprights to center both the heat pipe container and the shaft, which was concentric with the heat pipe container. A small pin was made from a 1.58 mm (0.0625 in) dowel pin, where one end was ground to 0.26 mm to fit in the base of the helical groove. This sprung pin was set in a hole in the shaft where it engaged one of the grooves, as shown in Fig. 2(*b*). An angular displacement transducer was mounted onto another piece of angle aluminum. A vertical 6.35 mm (0.25 in) dowel pin was placed in the angle aluminum to align with the angular displacement transducer shaft. The dowel pin was held by a collet installed in the milling machine spindle in order to fix the location of the displacement transducer. The shaft of the transducer was linked to the shaft within the heat pipe by three set screws. As the milling machine table moved the pipe over the stationary shaft, the pin followed the helical groove, causing the shaft to rotate. The angular displacement transducer measured this rotation. A multimeter was used to measure the output voltage of the angular displacement transducer. The distance of the table movement was $(s - s_1)$, which was read from

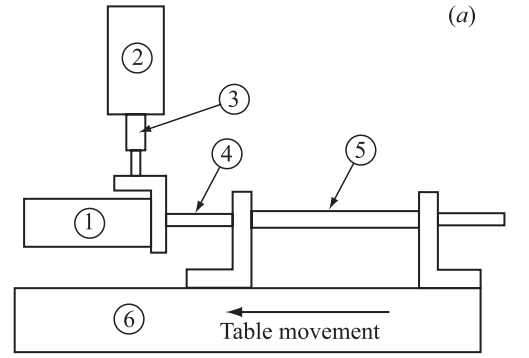

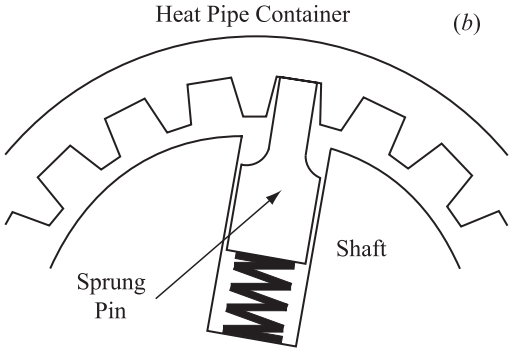

Figure 2. Schematic of the helical pitch measurement technique: (*a*) Major components; (*b*) Cross-sectional view of sprung pin engaging a helical groove.

the milling machine display unit. The transducer output voltage was measured over 10 cm lengths for ten different groups. Backlash errors were avoided by not reversing the table movement while taking data. The pitch was calculated using eqn. (7) at a point in the center of each 10 cm length. An average of 88 values were used to calculate the helical pitch.

Using the analysis given by Miller (1989), the root–sum–square uncertainties for the groove cross–sectional area, helical pitch, helix radius, groove length, groove volume, vapor space volume, and total mass of the working fluid inventory have been calculated. The measured and calculated uncertainties for all geometric variables presented are shown in Table 1.

A literature survey was completed to determine the specific volumes of ethanol vapor and liquid at various saturation temperatures, as shown in Fig. 3. This information was needed to determine the total mass and uncertainty of the working fluid inventory $m_t \pm \Delta m_t$. While existing texts report these properties (Faghri, 1995; Peterson, 1994, Lide and Kehiaian, 1994; Carey,

Table 1. The geometric variable values associated with the working fluid inventory.

Measured Values	
h	0.03831 ± 0.00076 cm
w	0.03445 ± 0.0010 cm
θ_1	$15.44° \pm 0.91°$
θ_2	$13.80° \pm 0.96°$
D_{vs}	1.359 ± 0.005 cm
L_t	43.8 ± 0.084 cm
Calculated Values	
A_{gr}	$1.703 \times 10^{-3} \pm 6.0 \times 10^{-5}$ cm^2
p	135.8 ± 5.9 cm
r_h	0.6992 ± 0.0025 cm
L_{gr}	43.82 ± 0.84 cm
V_{gr}	3.73 ± 0.13 cm^3

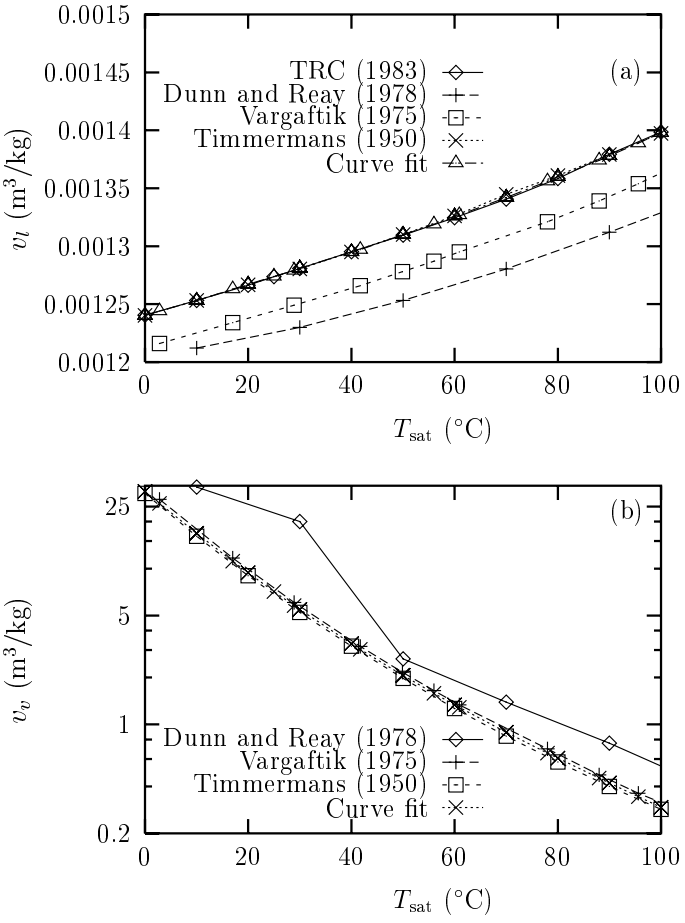

Figure 3. Specific volume of ethanol versus temperature: (*a*) Saturated liquid; (*b*) Saturated vapor.

1992; Schlunder, 1983; Ivanovskii et al., 1982), it was found that most simply referred to previous sources. Therefore, the data shown in Fig. 3 represent information gathered from primary sources that cannot readily be traced further. In Fig. 3(*a*), the available data for the specific volume of liquid in the range of T_{sat} = 0 to 100°C are relatively scattered. Vargaftik (1975) stated that the ethanol used was 96% pure by volume, with water making up most of the other 4%. Ethanol is agressively hygroscopic, so special procedures are required for further purification as outlined by Timmermans (1950) concerning anhydrous ethanol. Since the data by Timmermans (1950) and TRC (1983) are nearly coincident, it is believed that the data reported by TRC (1983) are also for anhydrous ethanol. Dunn and Reay (1978) do not provide information concerning purity. Therefore, the Vargaftik (1975) data and the Dunn and Reay (1978) data have been discarded in Fig. 3(*a*). In Fig. 3(*b*), the deviation of the Dunn and Reay (1978) data for the specific volume of vapor is significant. Therefore, the Dunn and Reay (1978) data has been discarded in Fig. 3(*b*). Polynomial curve fits from $0 \leq T_{sat} \leq 100$°C have been obtained for the data shown in Figs. 3(*a*) and 3(*b*) for the specific volumes of liquid and vapor ethanol. These curve fits have been evaluated at room temperature to determine the proper values to be used in the uncertainty analysis, since the heat pipe was filled at room temperature. Information concerning the uncertainty of the original data was not available. Therefore, the uncertainties of these properties have been estimated to be the maximum variance of the data from the curve fits ($\Delta v_l = 3.5 \times 10^{-8}$ m^3/kg, $\Delta v_v = 0.39$ m^3/kg). The specific volumes of liquid and vapor ethanol (m^3/kg) as functions of saturation temperature (°C) are shown below for the range $0 \leq T_{sat} \leq 100$°C

$$v_l = \exp(a_0 + a_1 T_{sat} + a_2 T_{sat}^2 + a_3 T_{sat}^3 + a_4 T_{sat}^4)/1000 \quad (8)$$

$$v_v = \exp(b_0 + b_1 T_{sat} + b_2 T_{sat}^2 + b_3 T_{sat}^3 + b_4 T_{sat}^4)/1000 \quad (9)$$

where the coefficients are

$a_0 = 0.2153$	$b_0 = 10.35$
$a_1 = 1.049 \times 10^{-3}$	$b_1 = -6.375 \times 10^{-2}$
$a_2 = -1.345 \times 10^{-8}$	$b_2 = 1.735 \times 10^{-4}$
$a_3 = 2.025 \times 10^{-8}$	$b_3 = 5.714 \times 10^{-7}$
$a_4 = -5.474 \times 10^{-11}$	$b_4 = -6.003 \times 10^{-9}$

The total mass of the working fluid inventory m_t and the associated uncertainty Δm_t for the range of fill values are given in Table 2.

Heat Pipe Filling Station

A filling station has been constructed which is capable of placing a low-temperature working fluid (i.e., water, ethanol,

Table 2. The calculated total mass of the working fluid inventory.

G	m_t (g)	Δm_t (g) Calculated	Δm_d (g) Filling Station
0.5	1.47	± 3.6%	± 5.0%
1.0	2.92	± 3.7%	± 2.9%
1.5	4.38	± 3.6%	± 1.9%

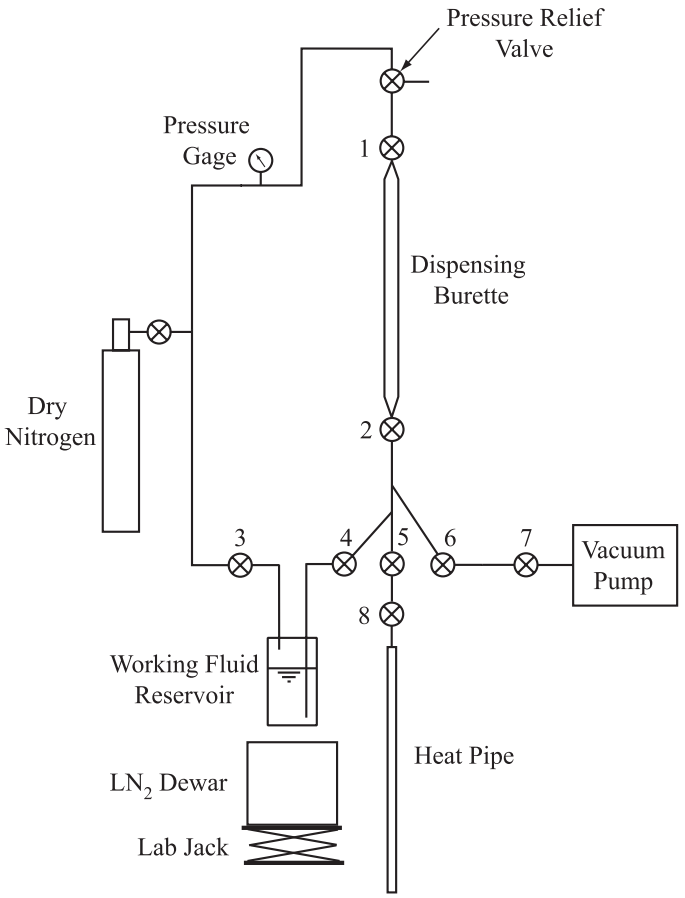

Figure 4. Schematic of the heat pipe filling station.

methanol) into a heat pipe without also introducing ambient air (Fig. 4). The station consisted of a manifold of valves and interconnecting stainless steel tubing, a working fluid reservoir, a dispensing burette, a vacuum pump, and a container of compressed dry nitrogen gas. Previous experience with filling stations showed that long runs of horizontal tubing could cause significant filling errors due to vapor bubbles within the tubing. To address this problem, the manifold was constructed such that the interconnecting tubing runs were very short (on the order of 2 cm). In addition, the tubes which intersect the main vertical tube between valves 2 and 5 (Fig. 4) were offset from each other and ran at a diagonal from the main tube. Again, the purpose of this design was to reduce the possibility of vapor bubbles adhering to the tubing walls, thus causing errors in the fill amount. However, it is likely that some vapor still does adhere to the tubing, so certain procedures were carried out during filling to eject as much vapor as possible. For instance, the 1 psig relief valve over valve 1 was cycled on and off several times. In addition, valves 2 and 5 were cycled on and off while noting the meniscus displacement within the dispensing burette. If the meniscus was displaced more than 0.06 cm^3, vapor was probably trapped within the valve. The valve in question was then cycled until the bubble was ejected.

To fill the heat pipe, the container was first evacuated to a pressure of 10^{-6} Torr using a turbomolecular vacuum pump. The sealed pipe was then connected to the filling station at valve 5. The working fluid was frozen and thawed repeatedly to reduce the amount of dissolved air within the fluid. The entire filling station was then evacuated by a roughing pump, except the working fluid reservoir. After evacuation, the liquid working fluid was drawn up into the dispensing burette and into all interconnecting tubing. After noting the height of the meniscus, the desired amount of working fluid was metered into the heat pipe by carefully opening the heat pipe fill valve 8. The difference in height of the liquid column was related to the dispensed mass of working fluid.

During initial testing of the filling station, it was found that the mass of working fluid dispensed into the heat pipe container was different than what was indicated by the dispensing burette. Therefore, a rigorous calibration of the filling station was undertaken to determine a correlation between the change in volume read by the dispensing burette and the change in mass of a receiving burette attached at valve 5, which was measured using a precision scale. The total uncertainty of the working fluid inventory dispensed by the heat pipe filling station Δm_d is given in Table 2.

Experimental Setup

The purpose of the experiment was to examine the steady–state performance of a helically–grooved copper–ethanol heat pipe under various heat inputs and transverse body force fields using a centrifuge table located at Wright–Patterson AFB (AFRL/PRPG). Specifically, the amount of working fluid was varied (G = 0.5, 1.0 and 1.5) to determine the effects of under/overfilling on the capillary limit, thermal resistance and evaporative heat transfer coefficient of the HGHP. To ensure uniform radial acceleration fields over the length of the heat pipe, the pipe was bent to match the radius of curvature of the centrifuge table (R = 1.22 m). Physical information concerning the heat pipe is given in Table 3. It should be noted that the total helix angle

Table 3. Helically–grooved heat pipe specifications.

Working fluid	Ethanol
Working fluid charge	m_t = 1.47, 2.92 and 4.38 g
Evaporator length	L_e = 15.2 ± 0.16 cm
Adiabatic length	L_a = 8.2 ± 0.16 cm
Condenser length	L_c = 15.2 ± 0.16 cm
Tube outside diameter	D_o = 1.588 ± 0.005 cm
Tube wall thickness	t_w = 0.0757 cm
Radius of curvature	R = 1.22 m
Wall/wick materials	Copper
Wick structure	Helical grooves
Number of Grooves	N_{gr} = 50
Heater element	Nichrome heater tape
Fill valve	Nupro B-4HW bellows valve
Calorimeter	1/8 in. OD coiled copper tubing

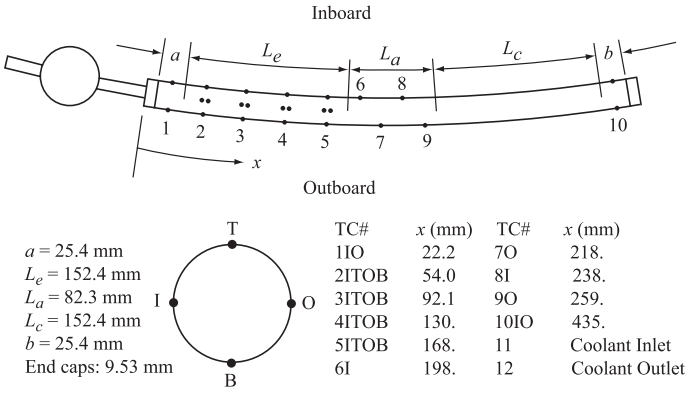

Figure 5. Thermocouple locations and relevant lengths.

was very small: Each groove rotated through an angle of approximately 2.03 rad (116 arc degrees) over the length of the pipe. The heat pipe was mounted to a platform overhanging the edge of the horizontal centrifuge table. This allowed the heat pipe to be positioned such that the radius of curvature was equivalent to the outermost radius of the centrifuge table. Insulative mounting blocks were used to ensure that the heat pipe matched the prescribed radius as closely as possible. The horizontal centrifuge table was driven by a 20-hp dc motor. The acceleration field near the heat pipe was measured by a triaxial accelerometer. The acceleration field at the centerline of the heat pipe radius was calculated from these readings using a coordinate transformation.

A pressure–sensitive nichrome heater tape with an aluminized backing was uniformly wound around the circumference of the evaporator section for heat input. Power was supplied to the heat pipe evaporator section by a power supply through power slip rings to the table. While the current reading could be made directly using a precision ammeter, the voltage across the electric heater had to be measured on the rotating table because of the voltage drop between the control room and the table. Therefore, the voltage at the heater was obtained through the instrumentation slip ring assembly and read by a precision multimeter.

The calorimeter consisted of a length of 1/8 in. OD copper tubing wound tightly around the condenser section. The size of the tubing was chosen to be small to minimize the effects of acceleration on the performance of the calorimeter. Thermal grease was used between the heat pipe and the calorimeter to decrease contact resistance. Type T thermocouples were inserted through brass T–branch connectors into the coolant inlet and exit streams, and a high-resolution digital flow meter was used to measure the mass flow rate of the coolant (50% by mass ethylene glycol/water mixture). The mass flow rate was controlled using a high–pressure booster pump, which aided the low–pressure pump in the recirculating chiller. The percentage of ethylene glycol was measured periodically during testing using a precision hydrometer to ensure that the mixture did not change. The temperature of the coolant was maintained at a constant setting by the recirculating chiller. Coolant was delivered to the centrifuge table via a double–pass hydraulic rotary coupling. The mass flow rate was constant for all experiments. Values of the specific heat of ethylene glycol/water mixtures were obtained from ASHRAE (1977), which were in terms of percent ethylene glycol by weight and temperature. The average temperature between the calorimeter inlet and outlet was used to evaluate the specific heat. The specific heat did not vary appreciably during testing since it is a weak function of temperature.

Heat pipe temperatures were measured by Type T surface–mount thermocouples, which were held in place using Kapton tape. Mounting locations for the thermocouples are shown in Fig. 5. A short unheated length next to the evaporator end cap was instrumented with thermocouples specifically for accurate thermal resistance measurements. In addition, groups of four thermocouples were arranged around the circumference of the heat pipe at stations in the evaporator section for local heat transfer coefficient information. Temperature signals were conditioned and amplified on the centrifuge table. These signals were transferred off the table through the instrumentation slip ring assembly, which was completely separate from the power slip ring assembly to reduce electronic noise. Conditioning the temperature signals prior to leaving the centrifuge table eliminated difficulties associated with creating additional junctions within the slip ring assembly. Temperature and acceleration signals were collected using a personal computer with data logging software. Since a shortage of thermocouple channels existed on the centrifuge table, a series of three electrical relays were engaged to read one set of thermocouples, and disengaged to read the other set.

Since the heat pipe assembly was subjected to air velocities due to the rotation of the table (up to 11 m/s = 25 mi/hr), efforts were made to reduce convective heat losses from the exterior of the heat pipe. A thin–walled aluminum box was fabricated to fit

Table 4. Maximum uncertainties of measured and calculated values.

Measured Values	
Coolant mass flow rate	$\Delta\dot{m}_c = \pm$ 0.05 g/s
Heater voltage	$\Delta V = \pm$ 0.5 V
Heater current	$\Delta I = \pm$ 0.1 A
Radial acceleration	$\Delta a_r = \pm$ 0.1-g
Calorimeter inlet temperature	$\Delta T_{\text{in}} = \pm$ 0.07 K
Calorimeter outlet temperature	$\Delta T_{\text{out}} = \pm$ 0.08 K
Evaporator end cap temperature	$\Delta T_{\text{eec}} = \pm$ 0.09 K
Condenser end cap temperature	$\Delta T_{\text{cec}} = \pm$ 0.11 K
Calculated Values	
Heat input	See Fig. 6
Heat transported	$\Delta Q_{\text{t}} = \pm$ 3.2 W
Thermal resistance	See Fig. 7
Heat transfer coefficient	See Figs. 12 and 13

around the heat pipe. Ceramic wool insulation was placed inside the box and around the heat pipe through three small doors on the top of the box. This insulation/box arrangement provided an effective barrier to convective losses from the heat pipe to the ambient.

The helically-grooved copper-ethanol heat pipe was tested in the following manner. The recirculating chiller was turned on and allowed to reach the setpoint temperature, which was measured at the calorimeter inlet. The centrifuge table was started from the remote control room at a slow constant rotational speed to prevent damage to the power and instrumentation slip rings. In this case, the radial acceleration was less than $|\vec{a}_r| < 0.01$-g. In all cases, the centrifuge table rotated in a clockwise direction as seen from above. Power to the heater was applied (Q_{in} = 10 W) and the heat pipe was allowed to reach a steady-state condition. The power to the heater was then increased to Q_{in} = 20 W and again the heat pipe was allowed to reach a steady–state condition. This was repeated until the maximum allowable evaporator temperature was reached ($T_{w,\max} = 100$°C). After all data had been recorded the power to the heater was turned off, and the heat pipe was allowed to cool before shutting down the centrifuge table.

Using the analysis given by Miller (1989), the uncertainties for all of the measured and calculated values for the experimental data are presented in Table 4.

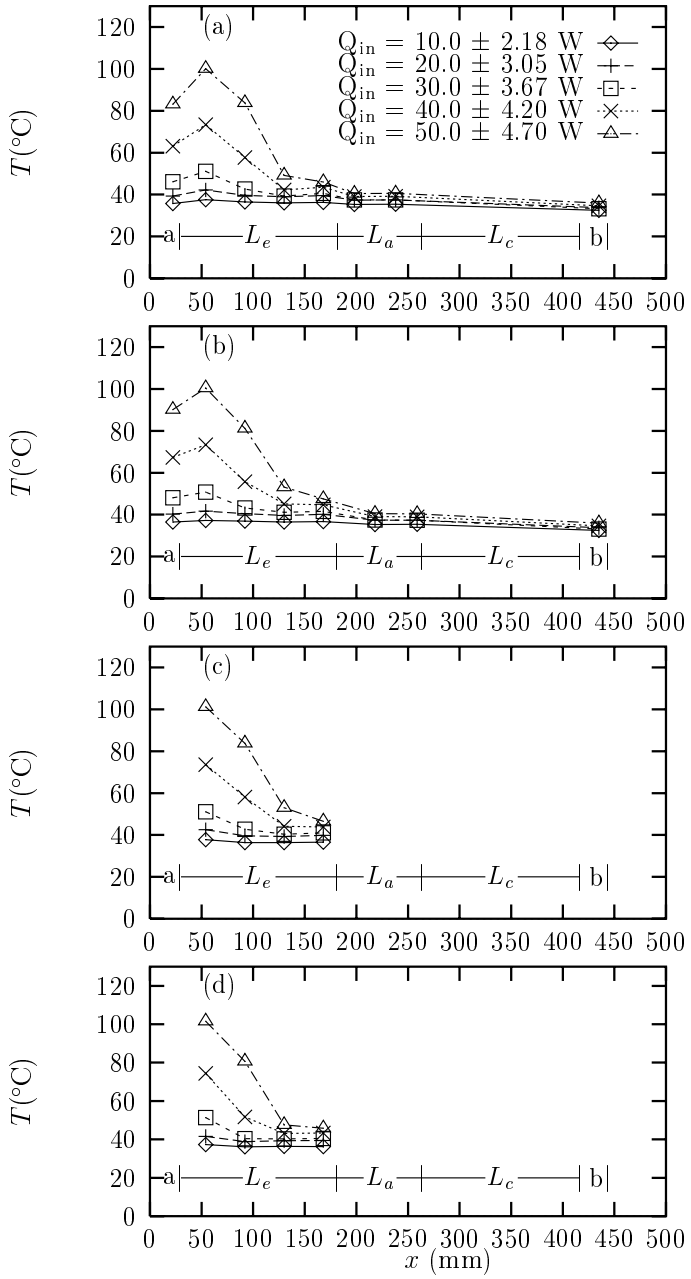

Figure 6. Steady–state temperature distributions for $|\vec{a}_r|$ = 0.01-g, G = 1.0: (*a*) Inboard; (*b*) Outboard; (*c*) Top; (*d*) Bottom.

Results and Discussion

The objective of this experiment was to determine the steady–state performance of a revolving helically–grooved heat pipe as a function of the working fluid inventory. The heat input, radial acceleration and working fluid fill were varied as follows: Q_{in} = 10 to 180 W, $|\vec{a}_r|$ = 0.01 to 10-g, and G = 0.5, 1.0 and 1.5. Thermocouples on the inboard, outboard, top, and bottom sides of the heat pipe (Fig. 5) were used to determine the axial and circumferential temperature distributions. Typical steady–state temperature distributions for the heat pipe for G = 1.0 at $|\vec{a}_r|$ = 0.01-g are shown in Fig. 6. For low power input levels, the temperature distribution was uniform. As the power input increased, the temperatures within the evaporator and the short unheated section adjacent to the evaporator increased significantly, indicating a partial dryout situation. Since the coolant temperature

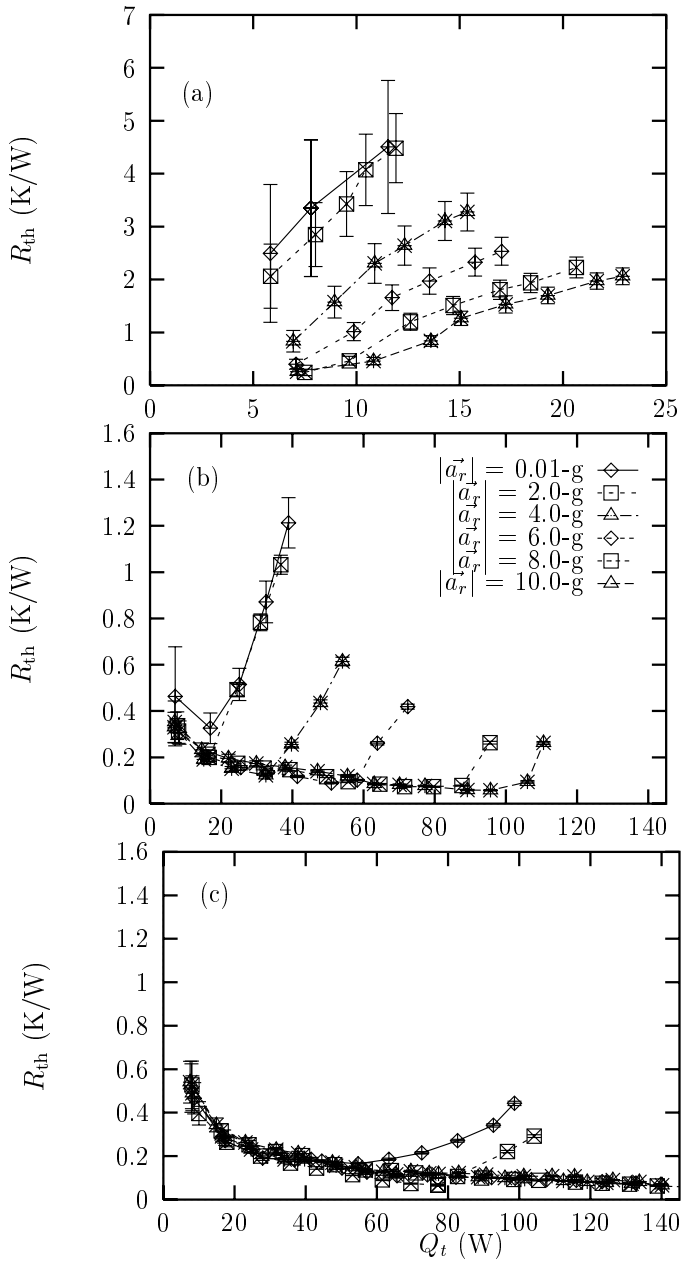

Figure 7. Thermal resistance versus heat transport: (*a*) G = 0.5; (*b*) G = 1.0; (*c*) G = 1.5.

and flow rate were constant for all tests, the adiabatic and condenser temperatures increased slightly with input power. Figure 7 shows the thermal resistance versus transported heat over the entire range of radial acceleration for each fill level. In Fig. 7(*a*) the thermal resistance was quite high, which indicates that the heat pipe was partially dried out for G = 0.5, even at the lowest power input levels. However, the thermal resistance decreased

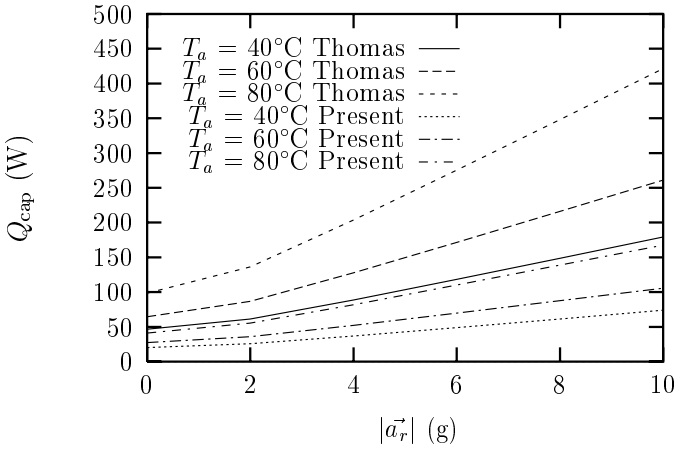

Figure 8. Capillary limit versus radial acceleration comparison of present model and Thomas et al. (1998).

significantly as the radial acceleration increased, showing that the capillary pumping ability of the helical grooves increased. For G = 1.0 and 1.5, the thermal resistance decreased and then increased with transported heat when dryout commenced. The G = 1.5 fill tests showed dryout occurring only for $|\vec{a}_r|$ = 0.01 and 2.0-g. Dryout was not reached for G = 1.5 with $|\vec{a}_r|$ = 4.0, 6.0, 8.0 and 10.0-g due to reaching the maximum allowable heater temperature. The capillary limit was considered to be reached when the thermal resistance began to increase.

Thomas et al. (1998) presented a mathematical model which predicted the capillary limit of a helically–grooved heat pipe subjected to a transverse body force. This model accounted for the geometry of the heat pipe and the grooves (including helix pitch), body force field strength, and temperature–dependent working fluid properties. This model was updated to include the improved measurements of the wick geometry and working fluid properties. The capillary limit versus radial acceleration is given in Fig. 8 for various working temperatures with the Thomas et al. (1998) model and the present model. The capillary limit increased steadily with radial acceleration and working temperature. The present model shows a significantly lower prediction for the capillary limit when compared to the Thomas model due to the improved geometric measurements and working fluid property equations.

Figure 9 shows a comparison of the experimental data and present analytical model for the capillary limit of a revolving helically–grooved heat pipe. No attempt was made to maintain a constant adiabatic temperature during the experiments. Therefore, the working fluid temperature in the model was set to the adiabatic temperature found experimentally. For G = 0.5, the heat pipe operated successfully only for $|\vec{a}_r| \geq$ 8.0-g. In Fig. 9(*b*) (G = 1.0), the capillary limit increased significantly with

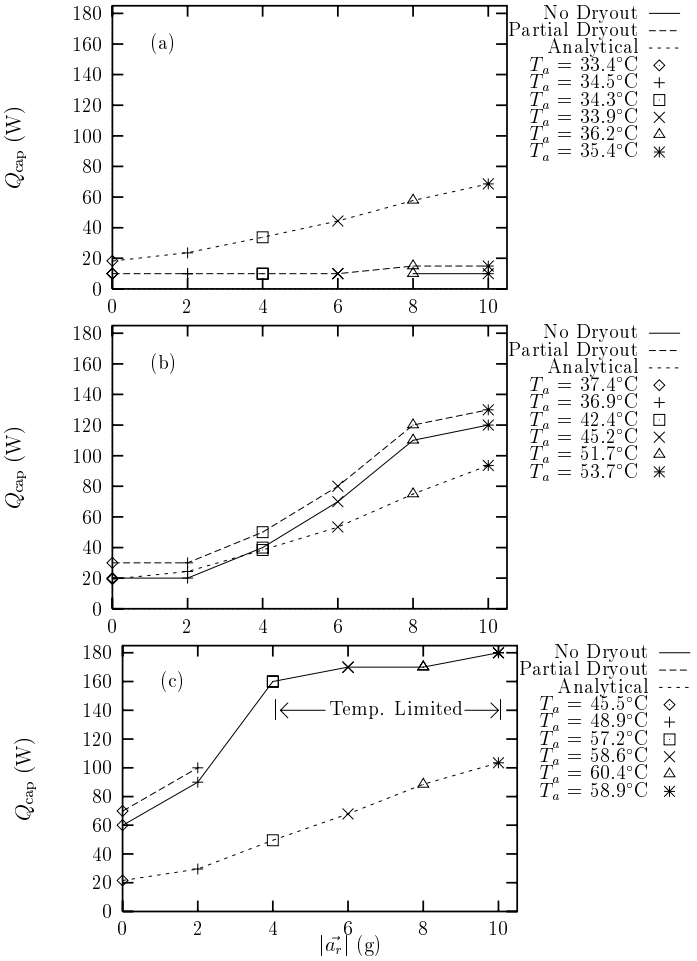

Figure 9. Comparison of present model and experimental capillary limit data versus radial acceleration: (*a*) *G*= 0.5; (*b*) *G* = 1.0; (*c*) *G* = 1.5.

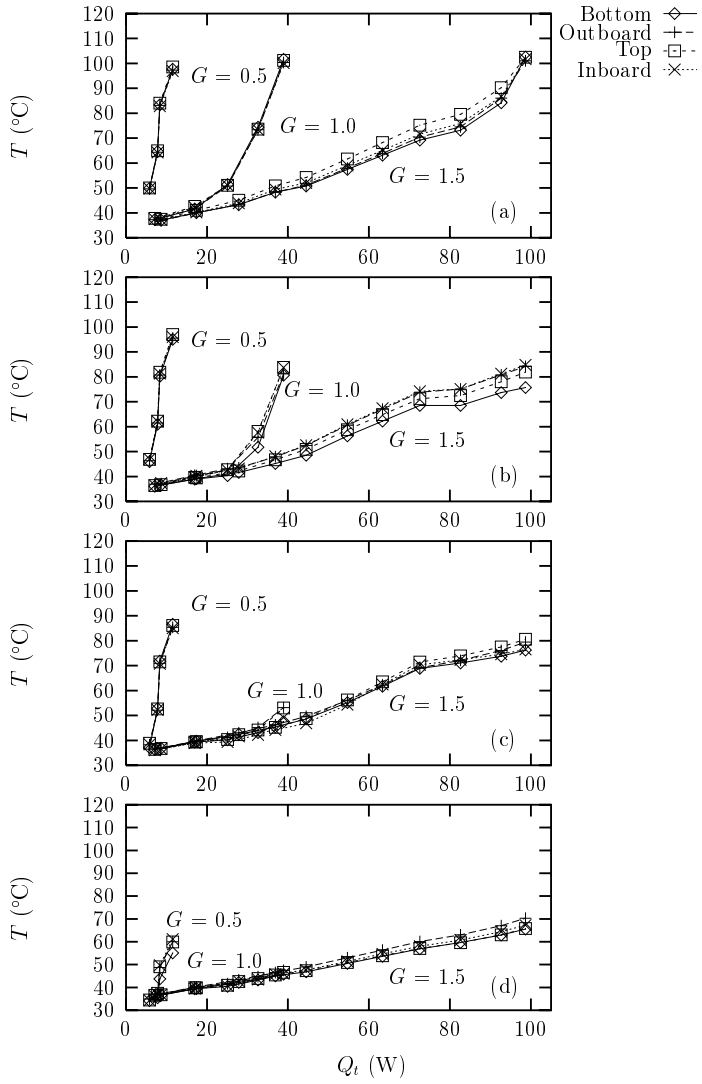

Figure 10. Temperatures within the evaporator section versus transported heat for $|\vec{a}_r| = 0.01$-g: (*a*) *x* = 54.0 mm; (*b*) *x* = 92.1 mm; (*c*) *x* = 130 mm; (*d*) *x* = 168 mm.

radial acceleration. With the heat pipe overfilled by 50% (*G* = 1.5), the capillary limit increased dramatically, showing the effect that overfilling has on performance. The agreement of the analytical model was very good for *G* = 1.0 as expected. For *G* = 0.5, the model overpredicted the experimental data because it was assumed that the grooves were completely filled. For *G* = 1.5, the model underpredicted the data due to the assumption that no liquid communication occurred between the grooves.

Temperatures within the evaporator section are shown in Figs. 10 and 11 for $|\vec{a}_r| = 0.01$-g and 10.0-g, respectively. In general, the temperatures within the evaporator increased with transported heat. In addition, the wall temperatures decreased with *G* for a given heat transport due to the fact that more grooves were active. The temperatures along the length of the evaporator section can be tracked by examining the case for *G* = 1.0. Near the evaporator end cap, the temperatures departed those for *G* = 1.5 at approximately Q_t = 15 W (Fig. 10(*a*)). At *x* = 92.1 mm (Fig. 10(*b*)), this departure was delayed until approximately Q_t = 25 W, and at *x* = 168 mm (Fig. 10(*d*)), the data for *G* = 1.0 and 1.5 were nearly coincident. This behavior shows that the grooves were essentially full near the adiabatic section, and proceeded to dry out closer to the evaporator end cap, as expected. Dryout for the *G* = 1.5 case can be seen in Fig. 10(*a*) where the temperatures converged to nearly the same value around the circumference. It should be noted that the temperatures around the circumference were relatively uniform for $|\vec{a}_r| = 0.01$-g. Evaporator temperatures for $|\vec{a}_r| = 10.0$-g are shown in Fig. 11. In comparison to $|\vec{a}_r| = 0.01$-g, the evaporator temperatures were in general lower due to the improved pumping ability of the helical grooves un-

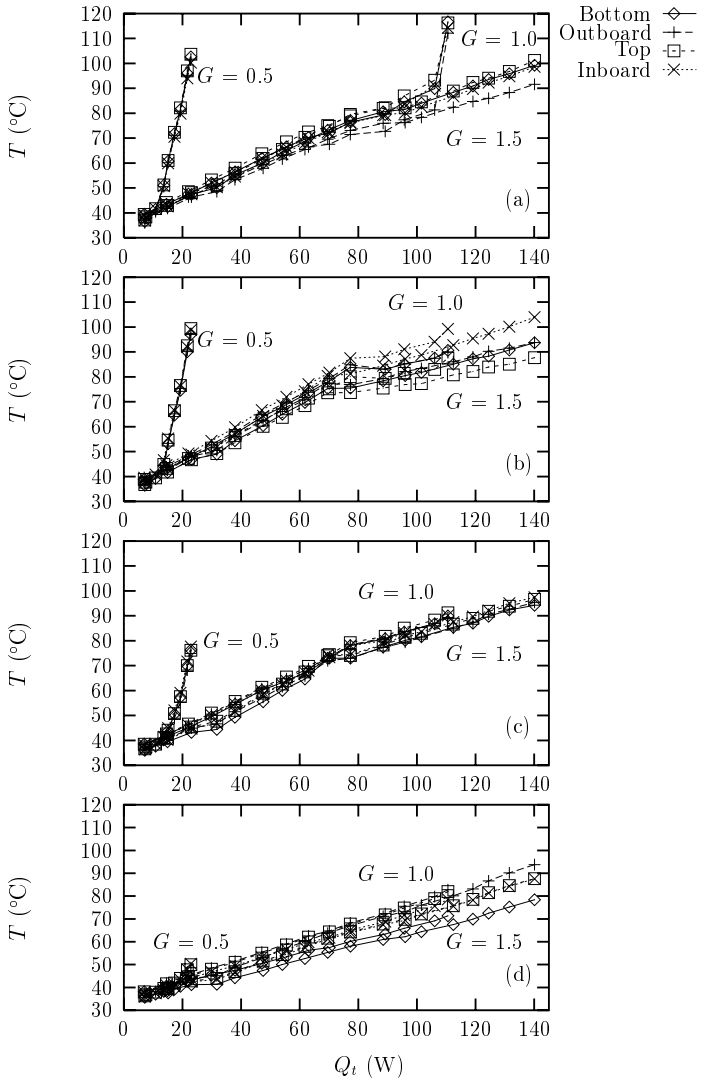

Figure 11. Temperatures within the evaporator section versus transported heat for $|\vec{a}_r| = 10.0$-g: (*a*) *x* = 54.0 mm; (*b*) *x* = 92.1 mm; (*c*) *x* = 130 mm; (*d*) *x* = 168 mm.

der increased radial acceleration. In addition, the temperatures tended to overlap over a greater range of heat transport values. In contrast to $|\vec{a}_r| = 0.01$-g, the evaporator temperature variation was greater around the circumference at higher Q_t, but no pattern was distinguishable in the data.

Local heat transfer coefficient data versus heat transport is shown in Figs. 12 and 13 for $|\vec{a}_r| = 0.01$-g and 10.0-g. Overall, the values for h_e were very low for G = 0.5 due to the fact that most of the grooves were dried out. As the percent fill increased from G = 0.5 to G = 1.0, the heat transfer coefficient increased significantly. For $|\vec{a}_r| = 0.01$-g (Fig. 12), h_e increased and then decreased with transported heat. This trend was also reported by Vasiliev et al. (1981) for an aluminum axially–grooved heat pipe with acetone as the working fluid. For G = 1.0 and 1.5, the heat transfer coefficient near the evaporator end cap (Fig. 12(*a*)) decreased until all of the values around the circumference converged. Closer to the adiabatic section, the heat transfer coefficient values around the circumference had not yet converged, showing these portions to still be active. For $|\vec{a}_r|$ = 10.0-g (Fig. 13), the values of h_e were significantly more uniform around the circumference and along the axial direction, even during a dryout event (G = 1.0, Fig. 13(*a*)). In addition, the heat transfer coefficient seems to be more constant with respect to the transported heat compared to $|\vec{a}_r| = 0.01$-g. During the experiments, the heat pipe working temperature was not constant, which resulted in changes in the specific volume of the liquid and vapor of the working fluid. Since the heat pipe was filled at room temperature, it was important to quantify the potential effects of the change in volume of liquid in the grooves with temperature. Figure 14 shows the variation of the percentage of groove volume occupied by liquid G with saturation temperature for the three fill amounts over the range of working temperatures seen in the experiments. The maximum percent difference was 2.7%, which was not deemed to be significant.

Conclusions

The effect of fluid inventory on the steady–state performance of a helically–grooved copper–ethanol heat pipe has been examined both experimentally and analytically. It was found that the capillary limit increased and the thermal resistance decreased significantly as the amount of working fluid within the heat pipe increased. In addition, the evaporative heat transfer coefficient was found to be a strong function of the fill amount. The updated analytical model was in very good agreement with the experimental capillary limit results for G = 1.0. However, the analytical model overpredicted the capillary limit data for G = 0.5 and underpredicted the data for G = 1.5.

Acknowledgements

Funding for this project was provided by the Air Force Research Laboratory (PRPG) under Grant F33615-98-1-2844, and by the Ohio Board of Regents. The authors would also like to acknowledge the technical assistance of Mr. Don Reinmuller.

References

ASHRAE, 1977, *Handbook of Fundamentals*, American Society of Heating, Refrigerating and Air–Conditioning Engineers, Inc., Atlanta, GA.

Brennan, P., Kroliczek, E., Jen H., and McIntosh R., 1977, "Axially Grooved Heat Pipes," *AIAA 12th Thermophsics Conf.*, Paper No. 77-747.

Carey, V., 1992, *Liquid-Vapor Phase-Change Phenomena*, Hemisphere, Washington, D.C.

Castle, R., 1999, "The Effect of Working Fluid Inventory on the Performance of Revolving Helically–Grooved Heat Pipes," Masters Thesis, Wright State University, Dayton, Ohio.

Dunn, P., and Reay, D., 1978, *Heat Pipes*, Pergamon, Oxford.

Faghri, A., 1995, *Heat Pipe Science and Technology*, Taylor and Francis, Washington, D.C.

Ivanovskii, M., Sorokin, V., and Yagodkin, I., 1982, *The Physical Principles of Heat Pipes*, Clarendon, Oxford.

Klasing, K., Thomas, S., and Yerkes, K., 1999, "Prediction of the Operating Limits of Revolving Helically–Grooved Heat Pipes," *ASME Journal of Heat Transfer*, Vol. 121, pp. 213–217.

Lide, D., and Kehiaian, H., 1994, *CRC Handbook of Thermophysical and Thermochemical Data*, CRC Press, Boca Raton, FL.

Miller, R., 1989, *Flow Measurement Engineering Handbook*, 2nd Edn., McGraw-Hill.

Peterson, G., 1994, *An Introduction to Heat Pipes: Modeling, Testing, and Applications*, Wiley, New York.

Schlunder, E., 1983, *Heat Exchanger Design Handbook*, Hemisphere, Washington, D.C.

Thomas, S., Klasing, K., and Yerkes, K., 1998, "The Effects of Transverse Acceleration Induced Body Forces on the Capillary Limit of Helically–Grooved Heat Pipes," *ASME Journal of Heat Transfer*, Vol. 120, pp. 441–451.

Timmermans, J., 1950, *Physico-Chemical Constants of Pure Organic Compounds*, Elsevier, New York.

TRC, 1983, *TRC Thermodynamic Tables—Non-hydrocarbons*, Thermodynamic Research Center: The Texas A & M University System, College Station, TX (Loose-leaf data sheets).

Vargaftik, N., 1975, *Handbook of Physical Properties of Liquids and Gases*, Hemisphere, Washington, D.C.

Vasiliev, L., Grakovich L., and Khrustalev D., 1981, "Low–Temperature Axially Grooved Heat Pipes," *Proc. 4th Int. Heat Pipe Conf.*, London, pp. 337–348.

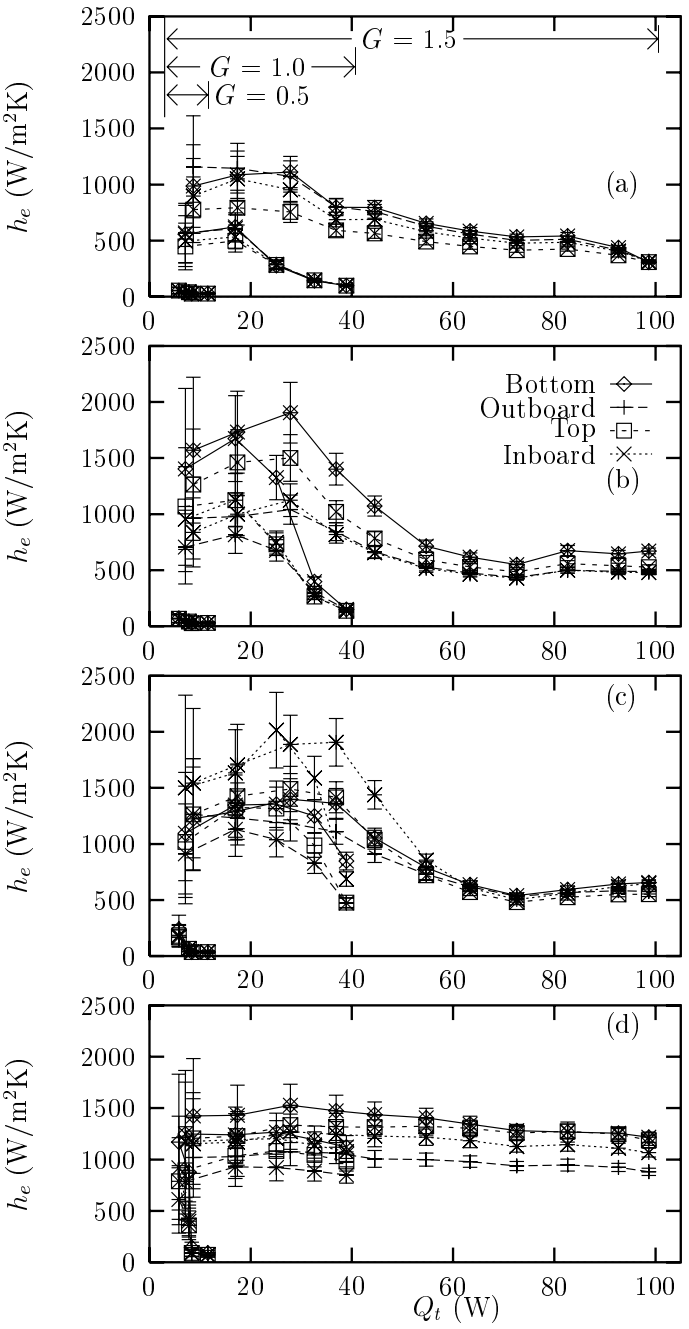

Figure 12. Heat transfer coefficients within the evaporator section versus transported heat for $|\vec{a}_r| = 0.01$-g: (*a*) *x* = 54.0 mm; (*b*) *x* = 92.1 mm; (*c*) *x* = 130 mm; (*d*) *x* = 168 mm.

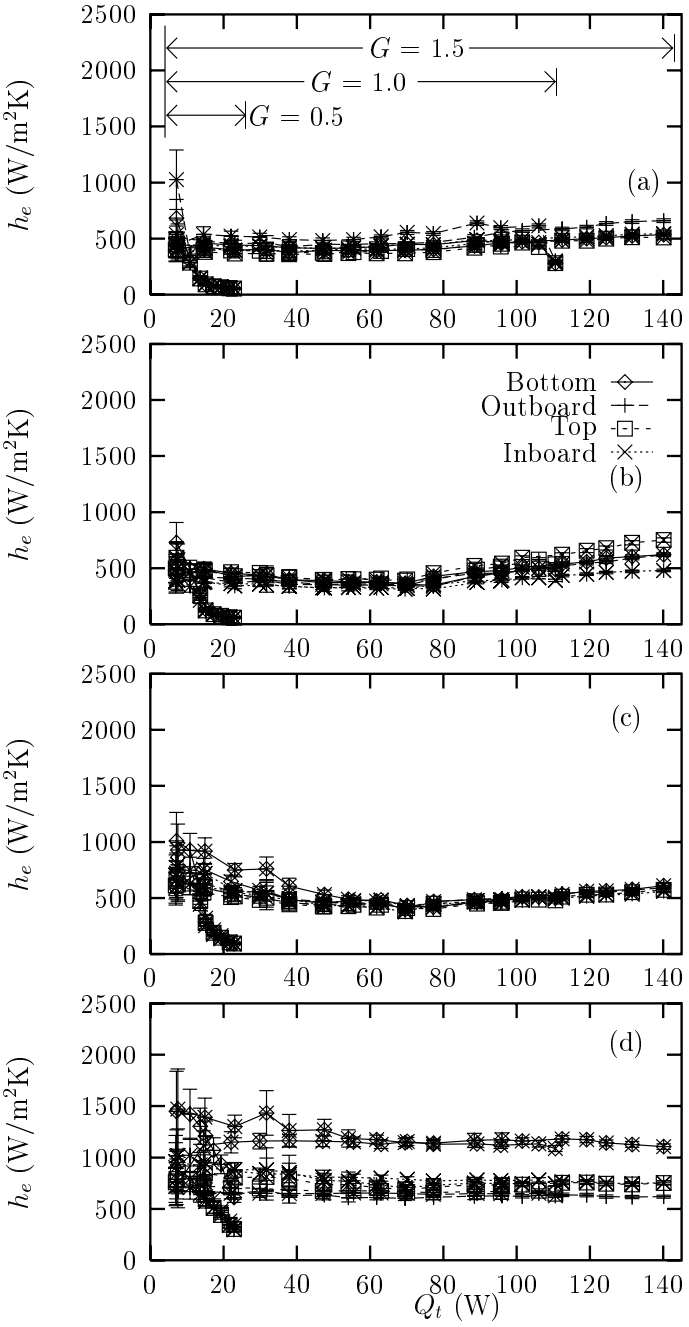

Figure 13. Heat transfer coefficients within the evaporator section versus transported heat for $|\vec{a}_r| = 10.0$-g: (*a*) *x* = 54.0 mm; (*b*) *x* = 92.1 mm; (*c*) *x* = 130 mm; (*d*) *x* = 168 mm.

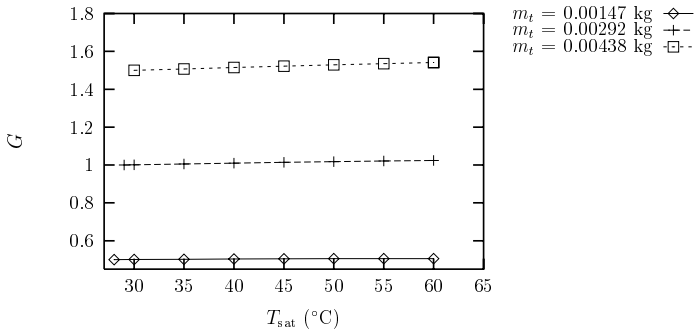

Figure 14. Ratio of liquid volume to total groove volume versus saturation temperature.